Proceedings of the Institution of Civil Engineers
**Engineering and Computational Mechanics 162**
March 2009 Issue EM1
Pages 11–21
**doi:** 10.1680/eacm.2009.162.1.11
**Paper EACM 700015**
Received 15/12/2007
Accepted 29/09/2008
**Keywords:** computational mechanics/mathematical modelling/ stress analysis

**John N. Karadelis**
Senior Lecturer, Department of Civil Engineering, Coventry University, UK

ice
Institution of Civil Engineers

# Concrete grandstands. Part II: numerical modelling

J. N. Karadelis MPhil(Eng), TEE

**This paper outlines the essential theoretical basis upon which a rigorous finite-element model comprising material non-linearities and failure criteria for both, concrete and steel reinforcement, is built. A numerical algorithm describing the analysis process, based on recent advances in numerical methods of reinforced concrete and a finite-element code were developed in parallel and summarised in a concise flowchart. It was concluded that the finite-element model captured successfully the non-linear flexural behaviour of the terrace units to failure, the formation of a 'bowl' at the centre, the lifting of the free tread ends and the rotation about a longitudinal axis. The results produced were rather sensitive to the modulus of elasticity assigned to concrete as well as the initial and, to a lesser extend, additional tangent moduli assigned to the reinforcement. The model was capable of predicting the introduction and propagation of flexural cracks formed around the midspan. More rigorous analytical and numerical work is under way, depicting both static and dynamic conditions, in an effort to establish suitable FE benchmarks, hence reducing uncertainties and increasing confidence of the performance of these structures during their working life.**

## NOTATION

| | |
|---|---|
| $E_c$ | modulus of elasticity of concrete |
| $f'_c$ | uniaxial compressive cylindrical stress |
| $f_{cu}$ | characteristic strength of concrete |
| $f_t$ | tensile strength of concrete |
| $I_1$, $I_2$, $I_3$ | first, second and third invariant of the stress deviator tensor |
| $J_1$, $J_2$, $J_3$ | first, second and third invariant of the stress tensor |
| $P_n$ | $n$th load step ($\forall n$: $n \in \aleph^+$) |
| $s_{ij}$ | deviator stress |
| $\delta_{ij}$ | Kronecker delta |
| $\bar{\varepsilon}$ | accumulated strain |
| $\varepsilon_{ij}$ | general strain tensor |
| $\varepsilon^e$, $\varepsilon^p$ | elastic and plastic strains respectively |
| $\sigma_{ij}$ | general stress tensor |
| $\sigma_m$ | hydrostatic mean stress |
| $\sigma_1$, $\sigma_2$, $\sigma_3$ | principal stresses |

## 1. INTRODUCTION: IDENTIFYING THE PROBLEM

Use of the finite-element (FE) method as a supplement to experiments and especially in situations where experimental work is either difficult to perform or cumbersome and expensive (e.g. reinforced concrete (RC) structures) has been increasing ever since the pioneering work of Ngo and Skordelis.[1] Extensive research has since resulted in significant advances in the area of constitutive concrete, leading to the development of a significant number of numerical models, partially listed in the reports of the American Society of Civil Engineers (ASCE) Committee on Finite Element Analysis of Reinforced Concrete Structures.[2]

The mechanical behaviour of RC as a composite material is not similar to that of its two basic constituents. Extensive research has, however, led to a few constitutive models for concrete based on the principles of continuum mechanics rather than the micro-mechanics of its molecular structure (crystallography). These models were based on the theory of elasticity following a linear or bilinear behaviour, or they incorporated a plasticity algorithm, or were capable of simulating plastic fracturing, or even a more general elasto-plastic behaviour.[3] This irregular behaviour of concrete as a material is attributed mainly to the following[4]

(*a*) the distinct non-linearity of its stress–strain path, especially in the near-peak domain, resulting from the development, growing and propagation of microcracks and the subsequent reduction in stiffness
(*b*) the softening tendency of concrete in the post-peak domain and the assemblage of these cracks in narrow bands
(*c*) the elastic stiffness dilapidation (decaying) caused by the successive opening and closing of cracks due to repeated loading–unloading
(*d*) the irrecoverable volume loss at high compressive loads resulting in an increase of Poisson's ratio.

Efforts will be directed in embracing most of the above in the numerical model presented below.

## 2. CONSTITUTIVE CONCRETE MODELS: THEORIES AND CRITERIA

Almost all classical theories of plasticity are based on five key concepts

(*a*) decomposition of strain into elastic and plastic parts
(*b*) yield criteria, determining the level at which yielding is initiated
(*c*) plastic flow rule, determining the direction of plastic strain

flow relative to $x$, $y$, $z$ axes and the relationship between stress and plastic strain under multiaxial loading

(*d*) strain hardening rule, describing and controlling the changes the yield surface undergoes with progressive yielding, so that the various states of stress, and the way in which resistance to plastic flow increases with plastic straining, can be established

(*e*) the unloading condition, demonstrating the irreversible behaviour of the solid.

Failure criteria are introduced to assess the possibility of failure of the material. As plastic strains develop, the yield surface increases in size while maintaining its original shape (isotropic, plastic behaviour) or moves to a different location within the material (kinematic hardening), or both.

Although the behaviour of concrete under complex stress conditions has been under investigation for many years, there is as yet no universally accepted constitutive law. Concrete in tension has been modelled in several ways, the most successful being a linear elastic and strain softening material—that is, the principal stresses and their directions are computed initially for an uncracked concrete. If the maximum principal stress exceeds a limiting value, a crack is assumed to form in a plane orthogonal to this stress. After the first crack the behaviour of that region of concrete becomes orthotropic. Linear and exponential mathematical models have been used to describe the descending part of the stress–strain diagram.

Concrete in compression is treated in a similar manner. The strength parameters, the tensile and compressive strength of concrete, are used to define the initiation of fracture by means of a tension 'cut-off' condition in the principal stress plane. When the combination of principal stresses violates this condition, a crack is initiated.

Failure theories represent states of stress and/or strain at which concrete can no longer sustain one of the criteria such as, yielding, load-carrying capacity, crack initiation and deformation, leading to rather complex failure curves and failure surfaces. The amount of experimental data needed for the implementation of such failure envelopes has, however, been limited until now.

Using index notation and terminology, the state of stress at a point inside a concrete element can be completely defined by the stress tensor, $\boldsymbol{\sigma}_{ij}$, in a three-dimensional (3D) stress system, where each component of the stress tensor acts on a surface normal to the $i$-axis and in the direction of the $j$-axis. In general, the stress tensor can be decomposed into two parts: the hydrostatic (mean) stress, $\boldsymbol{\sigma}_{\mathrm{m}}$, involving only pure tension and compression and the deviator stress, $\boldsymbol{s}_{ij}$, involving only shear, as follows

$$\boldsymbol{\sigma}_{ij} = \boldsymbol{s}_{ij} + \boldsymbol{\sigma}_{\mathrm{m}}\boldsymbol{\delta}_{ij} \tag{1}$$

where $\delta_{ij}$ is the Kronecker delta: $\delta_{ij} = \begin{cases} 1, & \text{if: } i = j \\ 0, & \text{if: } i \neq j \end{cases}$ (e.g. $\delta_{12} = 0$, but $\delta_{33} = 1$).

The condition for failure due to a multiaxial stress state is actually based on a model developed by Argyris,[5] who suggested a three-parameter criterion involving both stress invariants. Willam and Warnke[6] expanded on the Argyris model by adding two additional parameters, degrees of freedom (DOF), for describing meridian sections (surface generating curves) so that the failure surface model can be applied to low as well as high compression regions. Hence, they introduced a five-parameter criterion in which the tensile and compressive meridians were expressed by

$$\sqrt{\boldsymbol{I}_{2,\mathrm{t}}} = A_{01} + A_{11}\boldsymbol{J}_1 + A_{22}\left(\frac{\boldsymbol{J}_1^{\,2}}{\boldsymbol{f}_{\mathrm{c}}'}\right) \quad \text{tensile meridian } (\theta_{\mathrm{c}} = 0) \tag{2}$$

$$\sqrt{\boldsymbol{I}_{2,\mathrm{c}}} = B_{01} + B_{11}\boldsymbol{J}_1 + B_{22}\left(\frac{\boldsymbol{J}_1^{\,2}}{\boldsymbol{f}_{\mathrm{c}}'}\right) \quad \text{compressive meridian } (\theta_{\mathrm{c}} = 60^\circ) \tag{3}$$

where $A_{01}$, $A_{11}$, $A_{22}$, $B_{01}$, $B_{11}$, $B_{22}$ are constants, $\boldsymbol{f}_{\mathrm{c}}'$ is the uniaxial compressive cylindrical stress (straight meridians), $\boldsymbol{J}_1 = (\boldsymbol{\sigma}_1 + \boldsymbol{\sigma}_2 + \boldsymbol{\sigma}_2)$, the first invariant of the stress tensor and $\boldsymbol{I}_2 = \frac{1}{2}(\boldsymbol{s}_1 + \boldsymbol{s}_2 + \boldsymbol{s}_3)$ the second invariant of the stress deviator tensor

They were able to develop an expression for the failure curve by modelling it as part of an ellipse in the deviatoric plane. The five-parameter model was validated by utilising experimental data from Launay and Gachon.[7] It is characterised by a smooth surface and produces the main features of the triaxial failure surface of concrete. This is the criterion adopted by Ansys.[8]

In comparison, little work has been done in treating RC structures as 3D solids mainly because of the relative lack of knowledge of the concrete as a material under three-dimensional stress states. The most successful theory is probably attributed to Selby and Vecchio.[9] Their FE model used the secant stiffness (as opposed to tangent modulus) thus allowing for stability of the non-symmetric matrices developed but was only effective for short-term monotonic loads. Han and Chen[10] experimented with elasto-plastic constitutive models for concrete under triaxial states of stress. They used a hardening parameter in their non-uniform hardening plasticity model to simulate inelastic behaviour of concrete including brittle failure in tension, ductile behaviour in compression and volumetric dilatation under compressive loading. Their model could fit a wide range of experimental data, treating them as parameters such as shape factor, plastic modulus, modification factor and so on.

An alternative material model based on the theory of plasticity is that permitting dependence of strain on the loading history of the material. Hence, based on small strains theory, for multi-axial stress states and as irreversible material behaviour governs, the strain tensor can, in general, be decomposed into elastic and plastic strain increments such as

$$\mathrm{d}\boldsymbol{\varepsilon}_{ij} = \mathrm{d}\boldsymbol{\varepsilon}_{ij}^{\mathrm{e}} + \mathrm{d}\boldsymbol{\varepsilon}_{ij}^{\mathrm{p}} \tag{4}$$

## 3. STEEL REINFORCEMENT: ELASTO-PLASTIC BEHAVIOUR

For metals, including steel, the von Mises yield criterion with its associated flow rule and work (isotropic) hardening is adopted. For the case of reinforcement undergoing tension or compression, uniaxial conditions were assumed and a bilinear isotropic hardening approach was chosen to simulate the behaviour of steel. The material is assumed to undergo yielding when the equivalent stress reaches the yield stress. At the same time the corresponding yield surface depends solely upon the amount of plastic work done. It was therefore necessary to define and input the yield stress and a tangent modulus (gradient) after yielding, plus the modulus of elasticity and Poisson's ratio.

The final solution was obtained by utilising the linear solution, modified with an incremental and iterative approach. In general

$$\boldsymbol{\varepsilon}_n = \boldsymbol{\varepsilon}_{n(\text{ela})} + \Delta\boldsymbol{\varepsilon}_{n(\text{pla})} + \boldsymbol{\varepsilon}_{n-1(\text{pla})} \quad (5)$$

where $\boldsymbol{\varepsilon}_n$ is the total strain at the $n$th iteration, $\boldsymbol{\varepsilon}_{n(\text{ela})}$ is the elastic strain for the same iteration, $\Delta\boldsymbol{\varepsilon}_{n(\text{pla})}$ is the additional plastic strain obtained from the same iteration and $\boldsymbol{\varepsilon}_{n-1(\text{pla})}$ is the total and previously obtained plastic strain.

Convergence is achieved when Equation 6, is satisfied[11]

$$\left(\Delta\boldsymbol{\varepsilon}_{n(\text{pla})}/\boldsymbol{\varepsilon}_{n(\text{ela})}\right) < 0{\cdot}01 \quad (6)$$

This means that very little additional plastic strain is now accumulating and therefore the theoretical curve, represented by two straight lines (bilinear approach), is very close to the actual one.

## 4. NUMERICAL MODELLING

A step-by-step FE analysis (FEA) algorithm is developed in which provision is made for cracking and crushing of concrete (brittle failure) and the elasto-plactic behaviour of both materials, under static incremental loading conditions. A summary of the algorithm is shown in Figure 1.

### 4.1. Cracking and crushing of concrete

Based on the statements in Section 2, and assuming $\boldsymbol{\sigma}_1 \geqslant \boldsymbol{\sigma}_2 \geqslant \boldsymbol{\sigma}_3$, the failure condition of concrete could be divided into four discrete domains

(*a*) when $0 \geqslant \boldsymbol{\sigma}_1 \geqslant \boldsymbol{\sigma}_2 \geqslant \boldsymbol{\sigma}_3$, (i.e. compressive–compressive–compressive), crushing occurs
(*b*) when $\boldsymbol{\sigma}_1 \geqslant 0 \geqslant \boldsymbol{\sigma}_2 \geqslant \boldsymbol{\sigma}_3$, (i.e. tensile–compressive–compressive), cracking occurs
(*c*) when $\boldsymbol{\sigma}_1 \geqslant \boldsymbol{\sigma}_2 \geqslant 0 \geqslant \boldsymbol{\sigma}_3$, (i.e. tensile–tensile–compressive), cracking occurs
(*d*) when $\boldsymbol{\sigma}_1 \geqslant \boldsymbol{\sigma}_2 \geqslant \boldsymbol{\sigma}_3 \geqslant 0$, (i.e. tensile–tensile–tensile), cracking occurs.

As mentioned earlier, five input strength parameters are needed to define the failure surface, as well as a hydrostatic stress state. These are summarised in Table 1. The failure surface can be specified by a minimum of two constants, $\boldsymbol{f}_t$ and $\boldsymbol{f}_c$, whereas the other three constants default to specific values if the hydrostatic stress component, $\boldsymbol{\sigma}_m$, is low (all five parameters are needed if $\boldsymbol{\sigma}_m$ is high).[6]

### 4.2. Shear transfer

The discrete representation of reinforcement within the framework of the FE method is based on modelling the concrete and the reinforcing bars as different elements.

Ansys[8] recommends a 3D, eight-node, solid, isoparametric element (Solid65), with three translational DOF per node to simulate the nonlinear response of brittle materials such as concrete. For cracking in the tension zone the element includes a smeared crack analogy allowing cracks to be shown in the deformed shape. After the formation of the first crack, stresses tangential to the crack face may cause a second or third crack to develop and so on. The amount of shear transfer can be adjusted in the concrete material data table. This allows additional concrete material data such as tensile and compressive strengths and 'shear transfer coefficients' to be input in the program. The latter range from 0, representing a perfectly smooth crack with total loss of shear transfer, to 1, representing a perfectly rough crack with no loss of shear transfer. For crushing in the compression zone, it follows a typical plasticity law—that is, once the section has crushed any further application of load develops increasing strains at constant stress.

The element behaves in a linear elastic manner, if the applied tensile or compressive stress is less than the tensile or compressive strength of the material. If one of the applied principal stresses exceeds the tensile or compressive strength, however, then cracking or crushing of the element starts. Accordingly, cracked or crushed regions are formed perpendicular to the relevant principal stress direction. In the numerical routines the crack formation is achieved by the modification of the stress–strain relationships of the element, hence introducing a plane of weakness in the required principal stress direction.

It is stressed here that the numerical analysis routines incorporated in the program dictate that cracked or crushed regions (and single cracks) are formed perpendicular to the direction of the applied principal stress, which has just exceeded the corresponding tensile or compressive strength of the material. Hence, in a typical flexural test and at regions near the mid-span, cracks should appear vertical (see Figure 10 later) whereas at regions near the supports they should be inclined at an angle of approximately 45° to the horizontal.

### 4.3. The problem of smeared reinforcement

The reinforcement could be modelled as an additional smeared stiffness, distributed through the centroid of the element in 3D Cartesian system orientation. Up to three different rebar specifications may be defined this way. They can resist tension and compression but surprisingly, no shear. The problem does not seem to be fully alleviated with the usual remedies such as the introduction of discrete tie-strut (Link8), or beam (Beam4) elements connected to the solid elements (Figure 2). This is because the beam elements would allow the reinforcement to develop shear stresses but, as they are primarily linear elements, they would not go beyond yielding and therefore no plastic deformation of the reinforcement is possible. The link

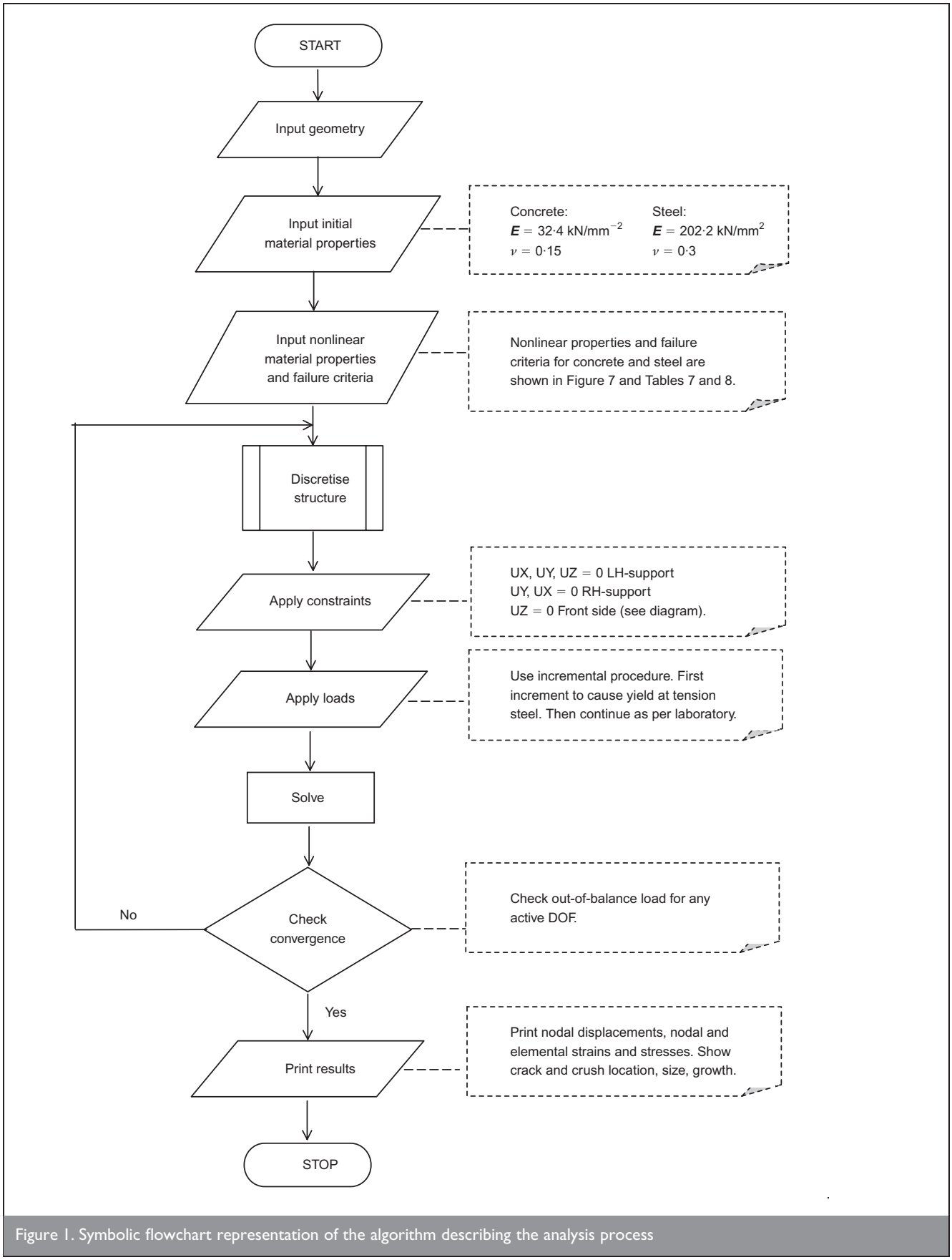


Figure 1. Symbolic flowchart representation of the algorithm describing the analysis process

elements, on the other hand, would allow elasto-plastic response of the reinforcement to be introduced in the RC simulation but, like the smeared reinforcement of the solid elements, no shear stress stiffness modelling is possible.

This problem can be averted by first considering the mechanism of shear transfer in a cracked concrete beam. This states that the applied shear stresses are resisted by the combined action of shear in the uncracked compression zone (approximately 30%), plus the contribution owing to aggregate interlock (approximately 45%), plus the dowel action of the longitudinal reinforcement (25%).[12] Taylor[12] demonstrated

| Parameter | Description |
|---|---|
| $f_t$ | Ultimate uniaxial tensile strength |
| $f_c$ | Ultimate uniaxial compressive strength |
| $f_{cb}$ | Ultimate biaxial compressive strength |
| $\sigma_H$ | Hydrostatic stress (ambient) |
| $f_1$ | Ultimate compressive strength for the state of biaxial compression superimposed on $\sigma_H$ |
| $f_2$ | Ultimate compressive strength for the state of uniaxial compression superimposed on $\sigma_H$ |

Table 1. Parameters used to define a failure surface (failure criterion by Willam and Warnke[6])

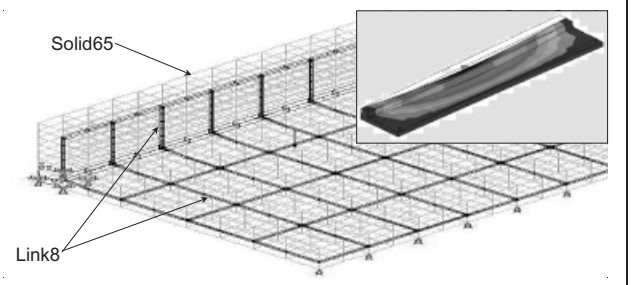


Figure 2. An FE model of a single terrace unit, steel elements are shown exaggerated for clarity. Inset: deformed shape of the unit, dark regions at the edges are virtually undeformed

that, as the applied shear force is increased, the dowel action is the first to reach its capacity after which a proportionally large shear is transferred to aggregate interlock.

The contribution the main steel (here modelled with Link8-elements) would therefore provide to shear resistance could be credited (passed) to the surrounding concrete and can even be specified for either both, open and closed cracks or one case only, as shown in Table 2. When cracking is imminent and the solution is converging to the cracked state, the modulus directly normal to the crack is significantly reduced and when the crack is open it is set to near zero. At this stage, the stiffness normal to the crack face will also be zero.

### 4.4. Softening of concrete

Concrete, unlike steel, shows a post-yield, strain-softening behaviour, obtained from routine tests on specimens such as cubes, cylinders, prisms and so on. This means that its stress–strain relationship follows a downward path after yielding. The traditional nonlinear solutions such as the Newton–Raphson (N–R), or modified Newton–Raphson (mN–R) techniques cannot handle such behaviour. This is because even zero stiffness at the unstable region (top of the curve, where the stiffness matrix changes its sign from positive to negative), possesses a problem for the N–R method. The latter becomes singular, inputted constraining equations become inadequate, the technique predicts an unbounded displacement increment and the model is declared unstable, often preventing further solution.

More recent advances promise solvers; they can offer sophisticated solution techniques such as Riks'[13] and Crisfield's[14,15] arc-length method. These solvers are incorporated in recent Ansys codes but they are bounded by restrictions such as only being suitable for certain elements and when the loading is strictly proportional; that is, where the load magnitudes are governed by a single scalar parameter. When the above is not the case, they do not obtain good results.

Attributing strain-softening characteristics to the post-peak behaviour of concrete seems, however, to be contradicting its brittle nature, especially when past studies have shown that strain softening is merely attributed to the interaction between specimen and loading platens of the apparatus.[16–18] In other words, if edge effects were eliminated, then concrete should be characterised by a complete and immediate loss of load-carrying capacity, as soon as its peak strength is reached. Hence, the well-known descending part of every laboratory-obtained concrete stress–strain curve is questionable, to say the least.

A series of laboratory tests, in a different research area, are currently being carried out at Coventry University on concrete beams and slabs with synthetic reinforcement. Although it is still too early for any firm conclusions it is, however, worth mentioning that the phenomenon of strain softening is absent, indicating that the softening effects may be attributed to the ductile behaviour of steel reinforcement and the composite action of the two materials.

### 4.5. Concrete–steel interaction

The transfer of forces across the interface between concrete and steel reinforcement by bond is of fundamental importance, as

| Shear transfer contribution as defined by Taylor[12]: % | For closed cracks: % | For open cracks: % | Ansys input. Closed cracks: shear transfer coefficient | Ansys input. Open cracks: shear transfer coefficient |
|---|---|---|---|---|
| Dowel action: 25 | 25 | 25 | 0·25* | 0·25* |
| Aggregate interlock: 45 | 45 | <45 | 0·40 + 0·25* | 0 |
| Compression zone: 30 | 30 | 30 | 0·3 | n/a |
| | | | Total: 0·95 | Total: 0·25 |

*Coefficient 0·25 (contribution of re-bars to shear transfer) is carried over.

Table: 2. Shear transfer coefficients and percentage of shear transfer attributed to concrete

flexural and other actions can cause the steel to slip through the concrete in a direction parallel to the bars. The interaction between concrete and steel is described by the assumption of a perfect bond. The latter is rather compatible with the smeared crack model from the point of view that no detailed description of the local effects is necessary. Also, as bond failure is a long process, the concrete material surrounding the reinforcement would probably have started departing the steel before the maximum bond stress is reached and any attempt to restrict these stresses to bond strength would be flawed. In any case, the detailed representation of the bond mechanism between steel and concrete is outside the scope of a macro/meso-scale mechanics model such as the present one.

Nevertheless, Link8 elements were embedded within the solid mesh by sharing common nodes with the Solid65 elements. In this case the unaided discrete representation of the reinforcement by one-dimensional, Link8 elements, connected to 3D, Solid65 mesh, was not made to account for possible displacement of the reinforcement relative to the surrounding concrete.

### 4.6. Computer simulation of laboratory tests

A series of comprehensive laboratory tests have been carried out elsewhere (Part I).[19] The aim was twofold. First, to investigate the behaviour of a family of RC terrace units supported at three positions and undergoing static, incremental loading. Second, to estimate the uncracked and fully cracked stiffness of the units. Two tests per unit were carried out for the latter aim. Test 1 assumed the section uncracked as it was transported from the factory and test 2 considered the same section, this time fully cracked, as received from test 1.

The geometry of the L-section terrace units and their design features are presented in Figure 3 and Tables 1, 2 and 3 of the companion part I paper.[19]

Figure 3 of the current paper shows the behaviour of typical concrete cylinders in uniaxial compression in accordance with the BS 1881,[20] its initial part being approximated by the 'best-fit' straight line. Softening, in this case, is regarded as a 'post-failure' phenomenon. The slope of the best-fit line was estimated to be 30·04 kN/mm$^2$.

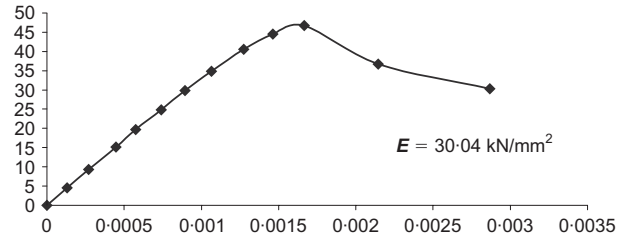


Figure 3. Stress–strain behaviour of grade C45 concrete in compression and estimation of its modulus of elasticity

Clearly, the correlation of test and numerical data depends a great deal on the assignment of accurate linear and nonlinear material properties, as appropriate. Hence, Young's modulus of concrete was related to its compressive strength by[21]

$$E_c = 9100\ (f_{cu})^{1/3} \quad (7)$$

In this case Hughes'[21] relationship yields a Young's modulus of 32·367 kN/mm$^2$ which is just 7·6% out of the average secant (static) modulus of elasticity value of 30·04 kN/mm$^2$ recorded in the laboratory. Also, it is less than 12·3% out of the average value of 28·80 kN/mm$^2$ obtained from ultrasonic laboratory tests and less than 3·4% out of 33·5 kN/mm$^2$, the value given by BS 8110.[22] These values are tabulated in Table 3. The value of 30·00 kN/mm$^2$ was adopted for FE modelling purposes.

The same British Standard for RC provides an estimate for its tensile strength based on its known compressive strength by

$$f_t = 0{\cdot}36\ (f_{cu})^{1/2} = 0{\cdot}36\left(\sqrt{45}\right) = 2{\cdot}42\ \ \mathrm{Nmm}^{-2} \quad (8)$$

The initial input properties for RC are shown in Table 4, whereas Table 5 was prepared to provide specific failure criteria for the concrete model.

Following the theory outlined in Section 3, the bilinear behaviour of deformed high-yield re-bars under tensile incremental loading was depicted in routine laboratory tests and is presented in Figure 4. The initial slope of the curve was taken as the elastic modulus of the material (198 kN/mm$^2$). Up to this point in the FE model the steel reinforcement is set to behave in a linear elastic manner. Plasticity is then introduced at a specified 0·2% proof stress (525 N/mm$^2$). The curve continues along the second slope defined by a tangent modulus (1·06 kN/mm$^2$). Failure occurs when the calculated value of stress reaches the ultimate value ($\sigma_u$= 660 N/mm$^2$) of the material. Failure criteria for steel in the form of stress and strain values are tabulated in Table 6.

The effect of self-weight of the terrace units was not taken into consideration when the laboratory tests were carried out—that is, for zero applied load the displacement was set to zero, although microcracks tend to develop in concrete at a very early stage, mainly owing to shrinkage. The same conditions for the theoretical model ensued.

### 4.7. Finite-element solution procedure

An essential feature of the nonliner solution strategy is the incremental application of load and the iterative procedure per load increment, hence the update of the stiffness matrix. In rate-independent material models these load steps take the role of the time steps. The computation of the state of strain and

| $E_{Hughes}$ | $E_{static}$ | $E_{ultrasonic}$ | $E_{BS8110}$ | $E_{FEA}$ |
|---|---|---|---|---|
| 32·367 | 30·04 | 28·80 | 33·5 | 30·00 |

Table 3. Moduli of elasticity values for concrete in kN/mm$^2$

| Concrete | | Steel re-bars | |
|---|---|---|---|
| $E_c$ | 30 kNmm$^{-2}$ | $E_s$ | 198 kN/mm$^{-2}$ |
| $f_{cu}$ | 45 Nmm$^{-2}$ | $f_y$ | – N/mm$^{-2}$ |
| $f_t$ | 2·42 Nmm$^{-2}$ | 0·2% proof stress | 525 N/mm$^{-2}$ |
| $\nu_{con}$ | 0·15 | $\nu_{steel}$ | 0·3 |

Table 4. Initial material properties as derived from design (see Table 3, Part I: experimental investigation[19]) and routine laboratory tests

| Failure criteria for concrete: stress (N/mm$^2$) | | | | | | | | |
|---|---|---|---|---|---|---|---|---|
| $\sigma_x$ (tens) | $\sigma_x$ (comp) | $\sigma_y$ (tens) | $\sigma_y$ (comp) | $\sigma_z$ (tens) | $\sigma_z$ (comp) | $\sigma_{xy}$ | $\sigma_{yz}$ | $\sigma_{zx}$ |
| 2·42 | −45 | 2·42 | −45 | 2·42 | −45 | 0·45 | 0·45 | 0·45 |
| **Failure criteria for concrete: strain** | | | | | | | | |
| $\varepsilon_x$ (tens) | $\varepsilon_x$ (comp) | $\varepsilon_y$ (tens) | $\varepsilon_y$ (comp) | $\varepsilon_z$ (tens) | $\varepsilon_z$ (comp) | $\varepsilon_{xy}$ | $\varepsilon_{yz}$ | $\varepsilon_{zx}$ |
| 0·0001 | −0·00175 | 0·0001 | −0·00175 | 0·0001 | −0·00175 | — | — | — |

Table 5. Failure criteria for concrete as inputted in the FE model

stress at a particular integration point (an interface the system uses to communicate with another application) is followed by a check against material failure. If failure is detected, then the type of failure (cracking–crushing), is established. Ansys[8] uses the smeared crack model for the representation of cracks with some advantages against discrete models, such as arbitrary directioning and no need for mesh adaptability and refinement. A drawback can be their disability to permit reliable description of the material behaviour in the vicinity of the crack and therefore only suited in macro-scale mechanics applications. Most of the smeared crack models reported in relevant literature are based on the theory of elasticity and only a small number of studies such as the one by Feenstra and de Borst[23] have reported plasticity models.

As plasticity is path dependent, it necessitates that, in addition to multiple iterations per load substep, the loads be applied slowly, in increments, with the presence of convergence tests in each substep, in order to characterise and model the actual (laboratory) load history. This is achieved by the NSUBST (number of substeps) command, defining the number of substeps to be taken within a load step. Ansys recommends a practical rule for load increment sizes, such as the corresponding additional plastic strain does not exceed the order of magnitude of the elastic strain. This can be achieved by applying additional load increments not larger than the load in step one, scaled by the ratio $E_T/E > 0{\cdot}05$. Such as

$$P_{n+1} = \frac{E_T}{E} P_n \qquad \forall n \in N \tag{9}$$

where
$P_{n+1}$ is the $(n+1)$th load step, $E$ is the elastic slope, $E_T$ is the plastic slope and $P_n$ is the $(n)$th load step.

Load substep one was chosen so as to produce maximum stresses approximately equal to the yield stress of the material. The yield stress was taken as 525 N/mm$^2$ from routine laboratory tests (Figure 4) and the corresponding load of 24·5 kN was noted. Also, the load to initiate yield was selected by performing a linear elastic analysis with a unit load and by restricting the stresses to the yield stress of the material. This was found to be approximately equal to 23·7 kN. The same design load at serviceability state conditions was 24 kN (Table 2, Part I).[19] In an effort to minimise uncertainties the number and size of successive load substeps were made to approximate the load history in the laboratory.

## 5. RESULTS AND DISCUSSION

### 5.1. Load–deflection

The experimental load-deflection response of unit 1 is reproduced in Figure 5, plotted along with the FE results. Test 1 represents the uncracked unit and test 2 the same unit cracked. It is clear from the path of the FE curve that the response of the model is linear until the first crack has formed at approximately 24 kN. This compares very well with the experimental findings. In test 2 (cracked unit) cracks inherited from test 1 have smoothened the overall behaviour of the unit.

The ultimate measured and predicted loads reached and the corresponding mid-span deflections are shown in Table 7. A large number of FE models depicting concrete behaviour predict deflections that are noticeably lower than the measured ones. This may be attributed, to a certain extent, to the plastic properties of the reinforcement, which can be such that converged solutions cannot be achieved beyond a certain load step, corresponding to a particular deflection value.

### 5.2. Strain variation

Figure 6 shows the measured and predicted strain variation at the lateral (SG1) and longitudinal (SG2) reinforcement at mid-span (Figure 6, Part I)[19] and Table 8 shows the ultimate strain values for both measured and predicted strains. All strain values are below the ultimate value of 3330 $\mu\varepsilon$. The strain

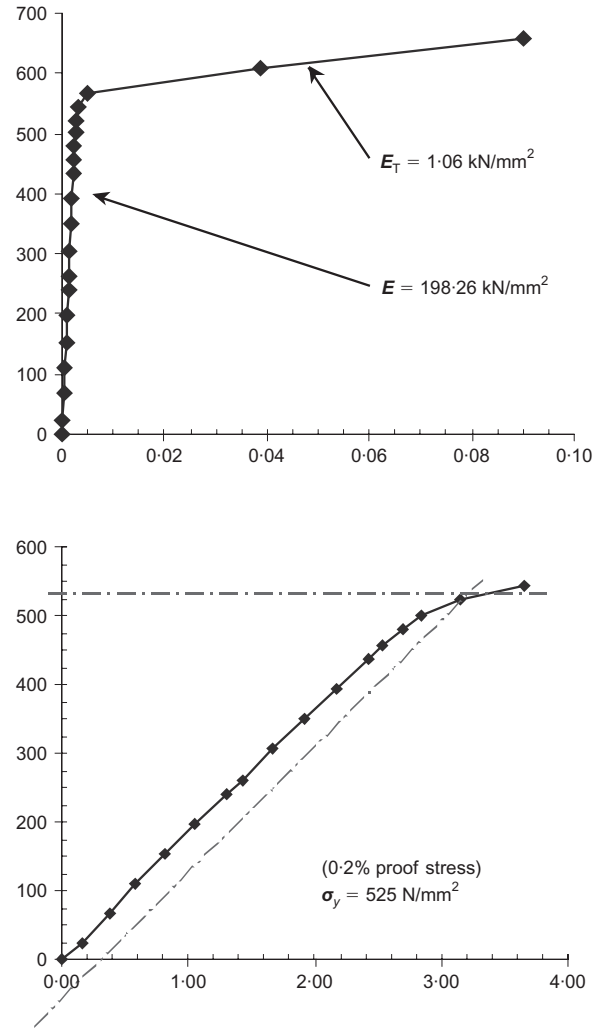


Figure 4. Stress–strain behaviour of type 2 high-yield steel reinforcement and determination of its modulus of elasticity and 'tangent' modulus

variation for the uncracked section is not depicted for reasons discussed earlier (see Section 4.4).

### 5.3. Flexural strain distribution

The distribution of strain across the depth of the riser at mid-span is shown in Figures 7 and 8. In order to facilitate a direct comparison, efforts were concentrated in harmonising, where possible, the load increments followed in the laboratory with those chosen by Ansys in the nonlinear analysis. The resemblance of the results obtained is very satisfactory (compare Figures 4 and 5, Part I).[19]

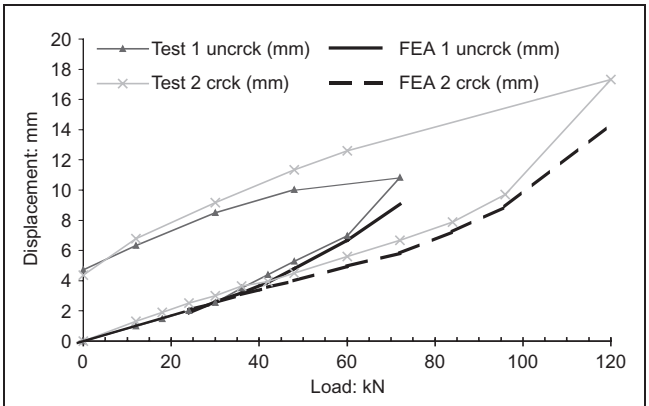


Figure 5. Comparison between measured and predicted displacements

| | Test 1 (uncracked unit) | Test 2 (cracked unit) |
|---|---|---|
| Measured ($W$, $\delta$): (kN, mm) | (72, 10·7) | (120, 17·2) |
| Predicted ($W$, $\delta$: (kN, mm) | (73, 9·08) | (126, 14·80) |

Table 7. Measured and predicted ultimate values of load and mid-span displacement

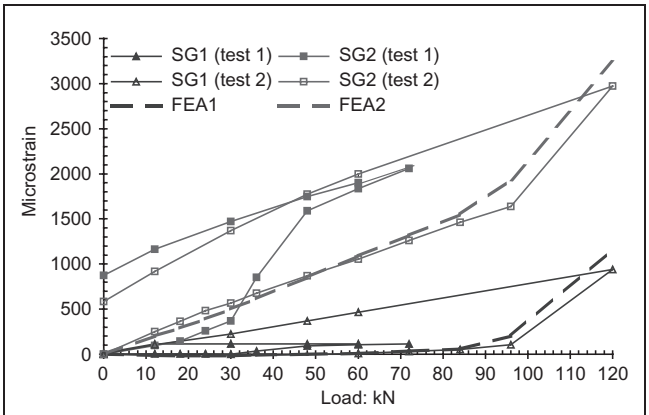


Figure 6. Comparison between measured and predicted strains developing at the reinforcement

In addition, the experimental crack formation at mid-span, Figure 9, compares well with the crack formation predicted by the FE model, shown in Figure 10. Cracking and crushing in Ansys are displayed by small circles and octahedra at locations

| Failure criteria for steel: stress (N/mm$^2$) | | | | | | | | |
|---|---|---|---|---|---|---|---|---|
| $\sigma_x$ (tens) | $\sigma_x$ (comp) | $\sigma_y$ (tens) | $\sigma_y$ (comp) | $\sigma_z$ (tens) | $\sigma_z$ (comp) | $\sigma_{xy}$ | $\sigma_{yz}$ | $\sigma_{zx}$ |
| 660 | −660 | 660 | −660 | 660 | −660 | — | — | — |
| **Failure criteria for steel: strain** | | | | | | | | |
| $\varepsilon_x$ (tens) | $\varepsilon_x$ (comp) | $\varepsilon_y$ (tens) | $\varepsilon_y$ (comp) | $\varepsilon_z$ (tens) | $\varepsilon_z$ (comp) | $\varepsilon_{xy}$ | $\varepsilon_{yz}$ | $\varepsilon_{zx}$ |
| 0. 09 | −0·09 | 0. 09 | −0·09 | 0·09 | −-0·09 | — | — | — |

Table 6. Failure criteria for steel as inputted in the FE model

| Lateral reinforcement | | Longitudinal reinforcement | |
|---|---|---|---|
| Test No: | (kN, με) | Test No: | (kN, με) |
| 1 | (72, 114) | 1 | (72, 2058) |
| 2 | (120, 940) | 2 | (120, 2974) |
| FEA1 | (126, 1167) | FEA2 | (126, 3238) |

Table 8. Measured and predicted ultimate values of load and mid-span strains

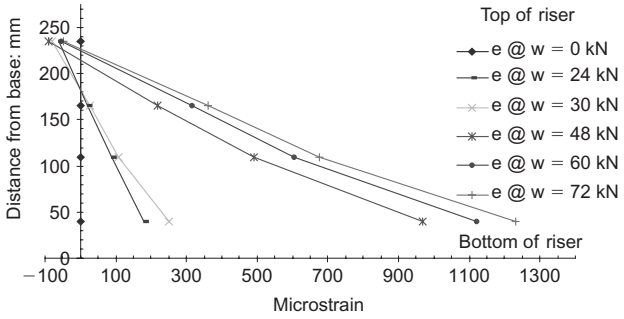


Figure 7. Unit 1, test 1. Predicted stress distribution across the depth of the riser

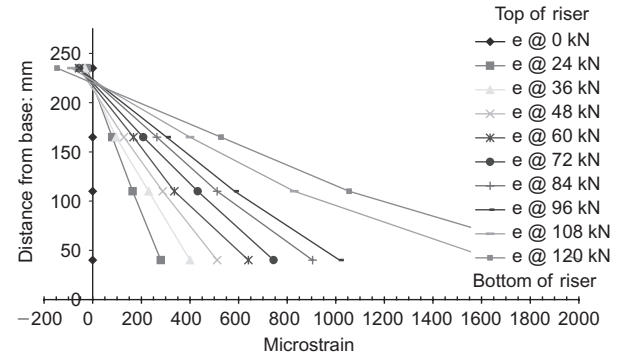


Figure 8. Unit 1, test 2, predicted stress distribution across the depth of the riser


Figure 9. Front view detail of the riser at mid-span, showing cracks developed in the laboratory

where concrete has cracked, or crushed respectively. If the crack has opened and then closed it is marked with 'x' through the circle. There is cracking evident in Figure 10, confirming that tension at the lower parts of the riser has been passed to the reinforcement.

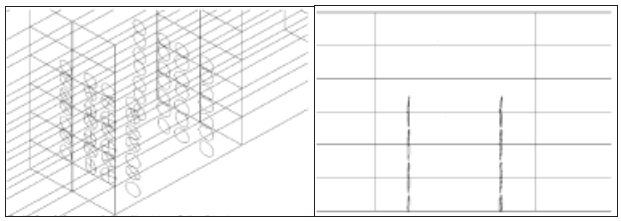

Figure 10. Isometric and front elevation (translucent view) details of the riser at mid-span showing predicted cracks by Ansys

### 5.4. Supplementary strain results

Finally, Figure 11 shows a comparison between measured and predicted strain readings for maximum load (72 kN) at specific positions on the surface of the terrace unit. It was shown, both experimentally and theoretically, that there was a gradual reduction in lateral compressive strain (and hence an increase in tensile strain) from the extreme support regions to the centre of the unit. This indicated an independent behaviour of the tread at the extremes and a similar behaviour to that of the riser near the middle. It also indicated the tendency of the unit to 'sink' in the middle and rotate about a horizontal longitudinal axis. In fact, the deformed FE model predicted a similar 'bowl' being deployed around mid-span and displayed torsional evidence of the unit about its longitudinal axis (inset, Figure 2). The tendency of the unit in the laboratory to leave the continuous support at the front and lift its corners has also been 'dramatised' by the computer, as nodal reactions were found negative (Figure 11).

Ansys provides a series of dedicated Contact elements that can model opening and closing, or sliding (friction) between two surfaces. These (nonlinear) elements would suit a condition such as lifting of the unit near the corners of the tread. If the emphasis of the analysis were at both the unit and the supporting medium, then best modelling practice would probably dictate the use of these elements. As, however, this is typical plate (slab) behaviour and as lifting can be clearly seen in the deformed shape of the FE model, it was decided that any more complex simulation of the interface between the UB-section, used as support, and the concrete unit should be unnecessary.

## 6. CONCLUSIONS

An accurate FE model of an RC terrace unit was developed in Ansys 7.0, by employing the dedicated concrete Solid65 and the Link8 elements and data obtained from a parallel laboratory investigation. The general elasto-plastic constitutive approach with the cracking and crushing options has captured successfully the nonlinear flexural behaviour of this composite unit to failure. The dedicated Solid65, 3D-element has been developed specifically for RC. No other element, including the family of powerful Shell (3D) elements, would be able to match the capabilities of the above and especially the modelling and prediction of cracks.

In general, 2D and Shell elements are best suited for 'membrane' or 'thin-walled' structures where the variation of stresses along the third dimension is either negligible, or of little interest. This is not the case with the (asymmetric cross-

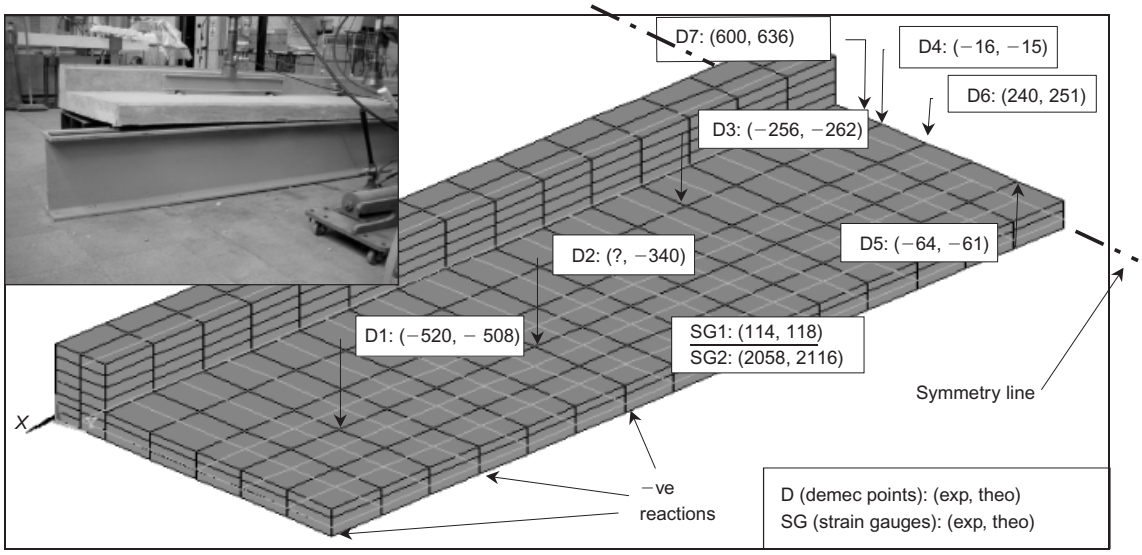


Figure 11. Unit 1, test 1, comparison between experimental and theoretical strains for maximum load of 72 kN at certain positions on the unit. D1, D2, D3, D4 are strains in the lateral, *y*-direction; D5, D6, D7 are strains in the longitudinal, *x*-direction. SG1 and SG2 are lateral and longitudinal strains developing on the reinforcement. Negative reactions, predicted by the FE model, are also shown in the inset, as lifting at the corners. All strains in $\mu\varepsilon$

section) terrace unit as its behaviour (bending and torsional effects, 'lifting' at the edges and 'sinking' at the centre) has shown. The use of solid elements will be reviewed at the next stage, when the whole grandstand is to be modelled.

The following conclusions can be made.

(*a*) The mode of failure predicted by the numerical model was of a flexural nature owing to increasing plastic strains developing in the tension zone (reinforcement). It was consistent with the experimental response.

(*b*) The FE model depicted accurately the formation of a 'bowl' at the centre of the unit and a 'region of inflexion' (change of sign of the bending moment values) surrounding it. The tendency of the tread to lift at the free ends (typical slab performance, noted during the experimental investigation) was also depicted by the numerical model, as corresponding node reactions were predicted negative. Finally, rotation of the units about a longitudinal axis was also captured.

(*c*) The results from the FE model were found to be rather sensitive to the modulus of elasticity assigned to the concrete as well as the initial and, to a lesser extent, additional tangent moduli assigned to the reinforcement. The various parameters controlling the nonlinear performance of the model are, however, numerous and mainly depend on the materials, geometry and the numerical techniques employed.

(*d*) It was found that in order to control the position of the reinforcement with accuracy and therefore achieve better results, it is necessary to simulate the latter in a discrete rather than smeared manner. Also, the inability of smeared reinforcement to transfer shear stresses discretely is still to be addressed. Hence, the development of dedicated elements is recommended. The Solid65 elements and the numerical models based on them can, however, be appropriate for simulating the main mode of failure of RC units.

(*e*) It is pointed out that although the FE model was capable of predicting the emergence of flexural cracks initiating at the bottom and propagating upwards, it was not suitable for predicting their length within the macro-scale mechanics domain. It could, however, be possible to estimate the width of the cracks, based on the elastic and plastic strain results obtained. Crack prediction and growth should be accompanied by good-quality graphics as the small circles used to represent cracks are disappointing and rather misleading.

(*f*) The experimental model was successfully simulated in the computer using nonlinear FEA and modelling techniques. In general, it has also been demonstrated that current methods and procedures of simulating, assessing, analysing and hence designing in RC can be improved. Further tests are required, combined with more rigorous analytical and numerical work and the establishment of benchmarks, in order to significantly reduce the uncertainties surrounding its performance during their working life.

The FE method is well suited to dealing with composite material models. Consequently, a constitutive RC model based on the theory of plasticity was developed, tested and discussed. One advantage of the theory of plasticity is the relatively simple and direct calibration of the state of stress. The latter results in the yield surface corresponding to a certain stage of hardening, having a strong physical meaning in relation to the strength envelop of concrete. Plasticity theory depends greatly on the existence of a yield surface. This statement is problematic when applied to concrete, as there has been a paucity of associated experimental data until now.

Finally, the choice of a well-established constitutive model in engineering research and practice is important as it affects accuracy. More experimental results and numerical models

dealing with complex stress states are necessary for research and general engineering applications in the future.

## REFERENCES


1. NGO D. and SKORDELIS A. C. Finite element analysis of reinforced concrete beams. *Journal of the American Concrete Institute*, 1967, **6**, No. 3 152–163.
2. ASCE TASK COMMITTEE. *Finite Element Analysis of Reinforced Concrete State-of-the-art Report*. American Society of Civil Engineers, New York, USA, 1982 and 1991.
3. AMERICAN SOCIETY OF CIVIL ENGINEERS (ASCE)/AMERICAN CONCRETE INSTITUTE (ACI) COMMITTEE 447. *Finite Element Analysis of Reinforced Concrete Structures* (ISENBERG J. (ed.)). ASCE, New York, USA, 1999.
4. BANGASH M. Y. H. Manual of numerical methods in concrete. *Modelling and Applications Validated by Experimental and Site Monitoring Data*. Thomas Telford, London, 2001, pp. 70–85.
5. ARGYRIS J. H. Recent developments in the finite element analysis of prestressed concrete reactor vessels. *Proceedings of an International Association for Bridge and Structural Engineering (IABSE) Seminar*, Istituto Sperimentale Modelli e Strutture (ISMES), Bergamo, Italy, 1974.
6. WILLAM K. J. and WARNKE K. Constitutive model for the triaxial behaviour of concrete. *Proceedings of an International Association for Bridge and Structural Engineering (IABSE) Seminar on Concrete Structures Subjected to Triaxial Stresses*, Part III-I, ISMES, Bergamo, Italy, 1974.
7. LAUNAY P. and GACHON H. Strain and ultimate strength of concrete under triaxial stress. *Proceedings of the 1st International Conference on Structural Mechanics in Reactor Technology (SmiRT), Berlin,* 1971, Paper H1/3. pp. 269–292.
8. *ANSYS 7·0. Elements and Theory Manuals*, ANSYS Inc., Canonsburg, PA, USA, 2002.
9. SELBY R. G. and VECCHIO F. J. A constitutive model for the analysis of reinforced concrete structures. *Canadian Journal of Civil Engineering*, 1997, **24**, No. 3, 460–470.
10. HAN D. J. and CHEN W. F. Constitutive modelling in analysis of concrete structures. *Journal of Engineering Mechanics*, 1987, **113**, 577–593.
11. WALZ J. E., FULTON R. E. and CYRUS N. J. Accuracy and convergence of FE approximations. *Proceedings of the 2nd International Conference on Matrix Methods in Structural Mechanics, Wright Paterson Air Force Base*, 1978.
12. TAYLOR H. P. J. The fundamental behaviour of reinforced concrete beams in bending and shear. *Proceedings of ACI–ASCE Shear Symposium*, Ottawa, 1973. (ACI Publication SP42) American Concrete Institute, Detroit, 1974, pp. 43–77.
13. RIKS E. *On the Numerical Solution of Snapping Problems in the Theory of Elastic Stability*. PhD thesis, Department of Aeronautics and Astronautics, Stanford University, 1970.
14. CRISFIELD M. A. A fast incremental/iterative solution procedure that handles snap through. *Computers and Structures*, **13**, 1981, No. 5, 55–62.
15. CRISFIELD M. A. *Non-Linear Finite Element Analysis of Solids and Structures. Vol. 1: Essentials*. Wiley, New York, 1991.
16. VAN MIER J. G. M. Multiaxial strain softening of concrete. *Materials and Structures*, RILEM, 1986, **19**, No. 111, 179–200.
17. VAN MIER J. G. M., *et al.* (TC148-SSC: Test methods for the strain softening of concrete). Strain softening of concrete in uniaxial compression. *Materials and Structures*, RILEM, 1997, **30**, No. 198, 195–200.
18. KOTSOVOS M. D., PAVLOVIĆ M. N. and COTSOVOS D. M. Structural concrete behaviour: separating myths from reality. *Proceedings of the 5th GRASM International Congress on Computational Mechanics, Limassol,* 2005, No. 1, 175–182.
19. KARADELIS J. N. Concrete grandstands. Part I: Experimental investigation. *Proceedings of the Institution of Civil Engineers, Engineering and Computational Mechanics,* 2008, **162**, No. 1, 3–9.
20. BRITISH STANDARDS INSTITUTION. *Testing Concrete. Recommendations for the Measurement of Dynamic Modulus of Elasticity*. BSI, London, 1990, BS 1881-209.
21. HUGHES B. P. *Limit State Theory for Reinforced Concrete Design*, 2nd edn. Pitman Publishing, London, 1976.
22. BRITISH STANDARDS INSTITUTION. *Structural Use of Concrete*. BSI, London, 1997, BS 8110 Part I.
23. FEENSTRA P. H. and DE BORST R., Aspects of robust computational modelling for plain and reinforced concrete. *Heron,* 1993, **38**, No. 4, pp. 1–76.